analytical chemistry

pubs.acs.org/ac Article

Label-Free Composition Analysis of Supramolecular Polymer–Nanoparticle Hydrogels by Reversed-Phase Liquid Chromatography Coupled with a Charged Aerosol Detector

Shijia Tang,*,▽ Zachary Pederson,▽ Emily L. Meany, Chun-Wan Yen, Andrew K. Swansiger, James S. Prell, Bifan Chen, Abigail K. Grosskopf, Noah Eckman, Grace Jiang, Julie Baillet, Jackson D. Pellett, and Eric A. Appel*

Cite This: https://doi.org/10.1021/acs.analchem.3c05747 Read Online

ACCESS | Metrics & More | Article Recommendations | Supporting Information

ABSTRACT: Supramolecular hydrogels formed through polymer–nanoparticle interactions are promising biocompatible materials for translational medicines. This class of hydrogels exhibits shear-thinning behavior and rapid recovery of mechanical properties, providing desirable attributes for formulating sprayable and injectable therapeutics. Characterization of hydrogel composition and loading of encapsulated drugs is critical to achieving the desired rheological behavior as well as tunable *in vitro* and *in vivo* payload release kinetics. However, quantitation of hydrogel composition is challenging due to material complexity, heterogeneity, high molecular weight, and the lack of chromophores. Here, we present a label-free approach to simultaneously determine hydrogel polymeric components and encapsulated payloads by coupling a reversed phase liquid chromatographic method with a charged aerosol detector (RPLC-CAD). The hydrogel studied consists of modified hydroxypropylmethylcellulose, self-assembled PEG-*b*-PLA nanoparticles, and a therapeutic compound, bimatoprost. The three components were resolved and quantitated using the RPLC-CAD method with a C4 stationary phase. The method demonstrated robust performance, applicability to alternative cargos (*i.e.*, proteins) and was suitable for composition analysis as well as for evaluating *in vitro* release of cargos from the hydrogel. Moreover, this method can be used to monitor polymer degradation and material stability, which can be further elucidated by coupling the RPLC method with (1) a multi-angle light scattering detector (RPLC-MALS) or (2) high resolution mass spectrometry (RPLC-MS) and a Fourier-transform based deconvolution algorithm. We envision that this analytical strategy could be generalized to characterize critical quality attributes of other classes of supramolecular hydrogels, establish structure–property relationships, and provide rational design guidance in hydrogel drug product development.

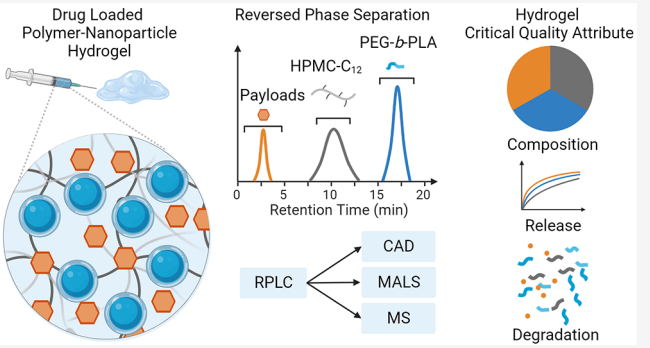

Supramolecular hydrogels are physically cross-linked viscoelastic biomaterials that are rapidly expanding in drug delivery, cell therapy, surgical coatings, medical device applications, and beyond.[1−10] Through tuning the chemistries and cross-linking density (mesh size of a hydrogel molecular network), hydrogels can be made to adopt vastly different chemical or physical properties and can encapsulate a variety of cargoes and accommodate different targeted release time frames.[3,6,7] In comparison to chemically cross-linked hydrogels, supramolecular hydrogels rely on physical, noncovalent interactions, such as ionic interactions, hydrophobic interactions, hydrogen-bonding, metal–ligand complexation, host–guest complexation, or biorecognition, which provide several clinical and process development benefits, such as gelation without reactive moieties or volume change.[1,6,10] Moreover, the reversible, noncovalent interactions in supramolecular hydrogels form dynamic and transient crosslinks, resulting in rapid self-healing and shear-thinning properties that make these hydrogels an ideal formulation strategy for sprayable and injectable therapeutics.[6,7]

While the materials library of supramolecular hydrogels is expanding, few analytical methods have been developed to characterize the critical quality attributes (CQAs) of hydrogels, such as drug loading, gel matrix composition (i.e. polymer content), and release profiles of the loaded drugs and polymers. Such attributes are important to establish hydrogel

Received: December 18, 2023
Revised: February 27, 2024
Accepted: March 18, 2024

Scheme 1. Supramolecular Polymer−Nanoparticle Hydrogel Composition and Gelation Process

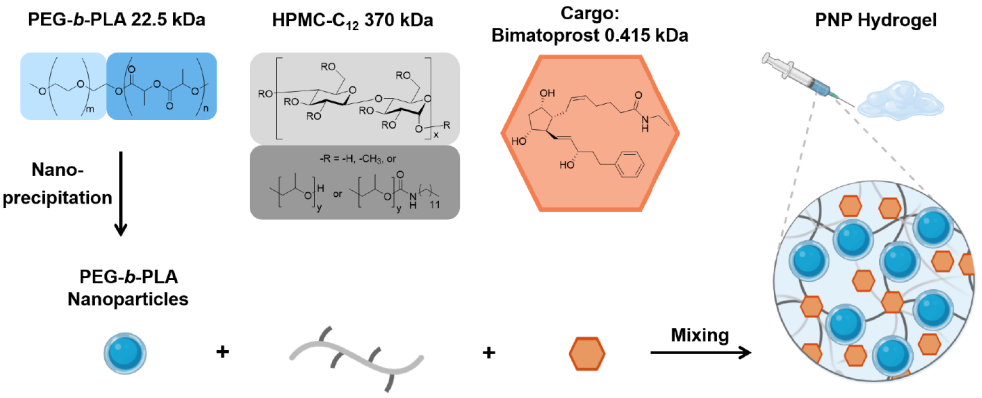

structure−property relationships and gain an understanding of the gelation process. For example, comparing polymer and drug release profiles simultaneously can shed light on the release mechanisms (*i.e.*, driven by diffusion and erosion), pharmacokinetics, and fate of the matrix polymers over time, and establish *in vitro* and *in vivo* correlation (IVIVC), thereby enabling the rational design of hydrogels for specific target product profiles.[3]

Several challenges are inherent to the composition analysis of supramolecular hydrogels. From a chromatography perspective, hydrogels often contain both encapsulated payloads and two or more high molecular weight and heterogeneous polymeric components as the gel matrix. This requires a method that resolves multiple components while allowing for good recovery for the polymers. In addition, an appropriate sample extraction procedure is critical to dissociate the supramolecular hydrogels and fully extract the individual components without degradation. As a result of these challenges, only the active payload is typically quantitated in hydrogel products to determine drug loading and release profiles.[11,12] Hydrogel degradation has been monitored gravimetrically (weighing a residual gel matrix), which provides limited information about the release of individual polymers and/or chemical changes (*i.e.*, molecular weight, degradation).[11−13] From a detection perspective, the encapsulated payloads are often UV active, while many polymers lack UV chromophores and require derivatization or an alternative detection principle to quantify. Labeling approaches, such as modifying the polymeric components with fluorescent tags or encapsulating fluorescent dyes as payload surrogates, have been developed for tracking the release of polymers and payloads from hydrogels.[14−20] However, labeling approaches can complicate hydrogel chemistries and release kinetics, depending on the degree of modification and the properties of the fluorescent modifiers. Tracking the fluorescence intensity may not fully reflect chemical changes in the polymer backbones over time. Identifying a label-free approach that combines chromatography separation with a universal detection technique for non-UV absorbing compounds would be beneficial to realize quantitation for all components in a supramolecular hydrogel and capture key chemical changes over time. However, label-free composition analysis of supramolecular hydrogels is rarely explored in the literature, and there remains a gap on what chromatographic separation modes and detection techniques can provide sufficient sensitivity, resolution, and recovery for all the components undergoing quantitative analysis.

Recently, a supramolecular hydrogel platform employing polymer−nanoparticle interactions between dodecyl-modified hydroxypropylmethylcellulose (HPMC-C_{12}) and poly(ethylene glycol)-*block*-poly(lactic acid) nanoparticles (PEG-*b*-PLA NPs) has been developed, which demonstrates injectability and rapid self-healing properties (Scheme 1).[21−26] These materials are denoted as PNP-*X*-*Y*, where *X* refers to the weight percent loading of the HPMC-C_{12} component and *Y* refers to the weight percent loading of the PEG-*b*-PLA NP component (*e.g.*, PNP-2-10 gels comprise 2 wt % HPMC-C_{12} and 10 wt% PEG-*b*-PLA NPs).

In this study, we use the PNP-2-10 hydrogel as a model system to develop a label-free analytical method utilizing reversed-phase liquid chromatography coupled to a charged aerosol detector (RPLC-CAD), which quantitates all components in the hydrogel: HPMC-C_{12}, PEG-*b*-PLA NPs, and an encapsulated therapeutic payload, bimatoprost. A C4 reversed-phase column was selected to provide specificity, sensitivity, and recovery for all of the hydrogel components. Due to the lack of UV chromophores on both polymeric components, a highly sensitive aerosol-based detection technique, CAD, was identified as most suitable to couple with the RPLC separation for quantitative analysis instead of differential refractometer or light scattering techniques. Beyond quantitation, the RPLC-CAD method was capable of differentiating polymer integrity after degradation or E-beam sterilization and could be combined with multi-angle light scattering (RPLC-MALS) or mass spectrometry (RPLC-MS) for further structural elucidation and monitoring of material stability. The method was also applicable to an alternative cargo, Bovine Serum Albumin (BSA), showing its generalization potential to characterize supramolecular hydrogels with various modalities of payloads. Our method demonstrated a label-free approach for composition analysis, characterizing degradation, and release profiles of supramolecular hydrogels, all of which are critical quality attributes.

EXPERIMENTAL SECTION

Materials and Reagents. USP grade HPMC, *N*, *N*-diisopropylethylamine, diethyl ether, hexanes, acetone, dimethyl sulfoxide (DMSO), dimethylformamide (DMF), acetonitrile (MeCN), *N*-methyl-2-pyrrolidone (NMP), 1,8-diazabicyclo(5.4.0)undec-7-ene (DBU), acetic acid, formic acid, monomethoxy-PEG (5 kDa), and 1-dodecyl isocynate were purchased from Sigma-Aldrich and used as received for polymers, nanoparticles, and hydrogel preparation. Lactide (LA) was purchased from Sigma-Aldrich and purified by

https://doi.org/10.1021/acs.analchem.3c05747
Anal. Chem. XXXX, XXX, XXX−XXX

recrystallization in ethyl acetate and sodium sulfate. Dichloromethane (DCM) was purchased from Sigma-Aldrich and further dried *via* cryo distillation. For size exlusion chromatography (SEC) and RPLC analyses, deionized water was obtained from an in-house Milli-Q water filtration system. Acetonitrile (MeCN) and tetrahydrofuran (THF) were purchased from JT Baker, and LC-MS grade trifluoroacetic acid (TFA) was purchased from Fisher Scientific. DMSO was purchased from Alfa-Aesar. Pullulan standards were purchased from the Polymer Standards Service. BSA was purchased from Thermo Fisher Scientific and bimatoprost was sourced from Toronto Research Chemicals.

Preparation of PNP Hydrogels. PNP-2-10 hydrogels were formulated (2 wt% HPMC-C_{12} and 10 wt% PEG-*b*-PLA NPs) according to the previous study.[26] "A 6wt% HPMC-C_{12} PBS solution was loadedinto a luer-lock syringe. Bimatoprost was added in a 20 wt% solution of NPs in PBS at the target concentration and was loaded into a separate luer-lock syringe. The NPs and HPMC-C_{12} syringes were connected througha female−female luer-lock elbow at each end separately. Care should be taken to avoid air at the interface of the HPMC-C_{12} and the NP solutions. The two solutions were mixed thoroughly until a homogeneous hydrogel was obtained.[26]

Instrumentation. The RPLC-CAD and SEC-CAD analysis used an Agilent 1260 series HPLC (Agilent Technologies, Santa Clara, CA) equipped with a quaternary pump, vacuum degasser, temperature controlled autosampler, thermostated column compartment, and diode array detector and coupled to a Thermo Dionex Corona Veo RS CAD detector (Thermo Fisher Scientific, Waltham, MA). For all analysis, CAD evaporation temperature was set to 35 °C, data collection was set to 5 Hz, and filter was set to 3.6 s.

Chromatographic Conditions for RPLC-CAD. The final optimized RPLC method used a Halo 400 Å C4 column. Mobile phase A (MPA) was 0.05% TFA (v/v) in water, and mobile phase B (MPB) was MeCN. The flow rate was 0.5 mL/min and column temperature was 60 °C. The sample diluent was 25% MeCN in water (v/v) unless otherwise stated. The final method gradient program was as follows: 0−2 min, initial hold at 25% MPB, 2−5 min, linear ramp from 25% to 80% MPB, 5−10 min, hold at 80% MPB, 10−11 min, linear ramp from 80% to 98% MPB, 11−15 min, hold at 98% MPB; then the gradient was brought back to the original condition. The thermostat temperature was set at 60 °C except for the E-beam experiment that was conducted at 50 °C.

PEG-*b*-PLA standards were prepared by dissolving the solid PEG-*b*-PLA polymer in MeCN at 1−2.5 mg/mL, then diluting with water or MeCN to achieve the desired concentration. In the diluent containing water, the PEG-*b*-PLA formed nanoaggregates and was denoted as PEG-*b*-PLA Agg (Figures S1, S2). HPMC-C_{12} standards were prepared by adding solid HPMC-C_{12} to 25% MeCN in water (v/v), then stirring until dissolved (1−2 h). Hydrogel samples were dissolved using the stepwise dilution as discussed in the Diluent Study section.

The chromatographic data were processed and analyzed in Empower (Waters, Milford, MA). Second order polynomial fitting was used for quantitation analysis against a multipoint calibration standard for each component.

Chromatographic Conditions for RPLC-MS. For MS analysis, an Agilent 1290 series HPLC (Agilent Technologies, Santa Clara, CA) equipped with a binary pump, vacuum degasser, temperature controlled autosampler, thermostated column compartment, and a diode array detector was coupled to an Agilent 6545XT qTOF. Chromatography conditions used the final method described above. Mass spectra were collected from 360 to 12 000 m/z at a rate of 3 scans/sec. The AJS source was set at a drying temperature of 325 °C, a capillary voltage of 3000 V, and a fragmentor voltage of 100 V. The molecular weight and repeating subunit analysis were conducted by deconvolving mass spectra from RPLC-MS total ion chromatograms with an open-source software iFAMS v.6.3 (iFAMS Quant), a Fourier-transform based algorithm developed by the Prell group to differentiate ion populations with high mass polydispersity (Figure S8).[27−31]

Method Validation. For specificity including forced degradation analysis, the HPMC-C_{12} (0.06 mg/mL) and PEG-*b*-PLA NPs (0.1 mg/mL) were stressed under acidic (0.1 M HCl, 25 °C), basic (0.1 M NaOH, 25 °C), and heated (60 °C) conditions for ∼20 h. The linearity was assessed over the range of 0.03−12 μg for HPMC-C_{12}, 0.01−5 μg for PEG-*b*-PLA, and 1−250 ng for bimatoprost. The linearity range was defined based on the nominal hydrogel sample composition. Accuracy and precision of each analyte was assessed at 10%, 100%, and 120% levels of the nominal sample loading. The average peak response and relative standard deviation (% RSD) were calculated for each analyte at each level (n = 3). Signal to noise was assessed at a sample loading of 0.03 μg for HPMC-C_{12}, 0.01 μg for PEG-*b*-PLA, and 1 ng for bimatoprost to determine the limit of quantitation (LOQ).

RESULTS AND DISCUSSION

Separation of Hydrogel Components by SEC and RPLC. The supramolecular PNP hydrogel contains components with vastly different molecular weights, conformations, and hydrophobicities (Scheme 1). The encapsulated cargo bimatoprost is a small molecule (Log P= 3.2). HPMC-C_{12} is a water-soluble, hydrophilic polymer with hydrophobic modifiers. PEG-*b*-PLA is an amphiphilic block copolymer and can self-assemble to form nanoparticles by a nanoprecipitation process, driven by the hydrophobicity of PLA. The PEG-*b*-PLA NPs consist of PLA segments as the core and PEG surface. We first focused on identifying a separation mode that could resolve and provide good recovery for all three components. Size based separation methods including SEC, hydrodynamic chromatography, and field-flow fractionation are powerful in polymer and nanoparticle analysis.[32−35] SEC is widely applied for polymer characterization, which separates analytes based on their hydrodynamic radius, R_h.[36] We assessed three SEC columns composed of hydrophilic polymer beads designed for the separation of high Mw water-soluble polymers by connecting them to a CAD (Table S1). Figure 1a displays a representative SEC-CAD chromatogram obtained by using the TOSOH TSKgel G5000PWXL. A sufficient resolution could be achieved among the four pullulan sizing standards (1330 kDa to 0.99 kDa) in the Mw range of the hydrogel polymers. However, HPMC-C_{12} and PEG-*b*-PLA NPs showed coelution in the SEC (Figure 1a). We investigated the coelution by coupling SEC to MALS and an inline viscometer (IV) to determine Mw and R_h. The IV analysis revealed that the HPMC-C_{12} and the PEG-*b*-PLA NPs had similar R_h (Table S2, Entry 1, 4), which, combined with the apparent high dispersity of HPMC-C_{12} (peak width ∼10 min at baseline), suggested that the resolving power of SEC was insufficient for hydrogel composition analysis.

This SEC study also elucidated that the PEG-*b*-PLA polymer rapidly and spontaneously formed aggregates in the

https://doi.org/10.1021/acs.analchem.3c05747
Anal. Chem. XXXX, XXX, XXX−XXX

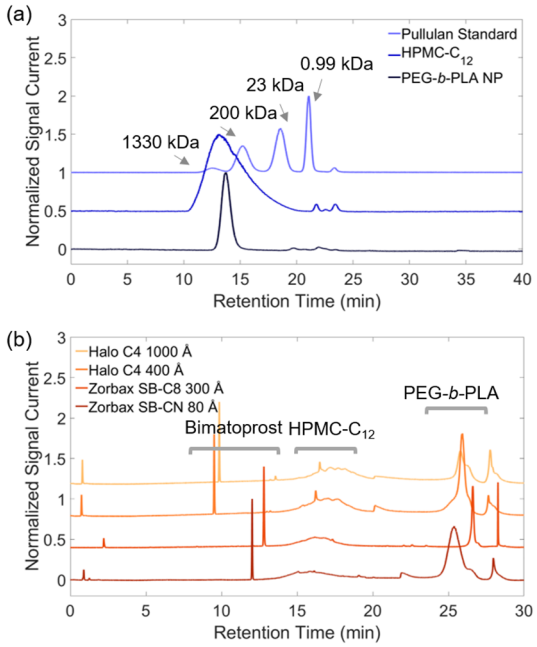

Figure 1. Representative chromatograms of bimatoprost, HPMC-C_{12}, and PEG-*b*-PLA NPs using different separation principles: (a) SEC-CAD and (b) RPLC-CAD.

SEC condition and in organic/aqueous mixtures such as the HPLC diluent (Figure S1). Before injection, when the PEG-*b*-PLA polymer was dissolved in 100% MeCN, no aggregates were detected by DLS (Figure S2a). After injecting the polymer solution in SEC, the Mw increased from 22.5 kDa as a single polymer chain to ~11 MDa with a hydrodynamic radius of 15.5 nm, indicating the formation of nanosized aggregates (PEG-*b*-PLA Aggs) spontaneously in the SEC condition (Table S2, Entry 3). The rapid aggregation of PEG-*b*-PLA polymers in an HPLC diluent was also detected by DLS (diameter = 31 nm) upon adding water into the polymer/MeCN solution, which mimics the polymer aggregation during HPLC sample preparation (Figure S2a). Due to the fast aggregation kinetics of the polymers in diluent or SEC conditions, the PEG-*b*-PLA NPs or Aggs were injected as-is in the following studies without destabilizing with organic solvents. Also, the comparable R_h, chemical composition, and formation process of the PEG-*b*-PLA Aggs and the PEG-*b*-PLA NPs suggested that the Aggs can be used as the external standard to quantify the NPs. In the following discussion, "PEG-*b*-PLA NPs" are used universally for both NPs and Aggs.

Since HPMC-C_{12} and PEG-*b*-PLA NPs have similar sizes, reversed-phase (RP) separation was selected to leverage the analytes' hydrophobicity differences to achieve selectivity. Reversed-phase is a less common separation mode for nanoparticle characterization because the small pore sizes of the column packing materials may not allow good recovery. This was of particular concern since the PEG-*b*-PLA NPs would be injected as-is without dissociation into individual polymers in the diluent. To promote the elution of HPMC-C_{12} and PEG-*b*-PLA, RP columns with 80−1000 Å pore sizes and less hydrophobic stationary phase chemistries were evaluated (Table S1). Figure 1b shows a comparison of four RP columns using a generic linear gradient with a thermostat temperature of 30 °C. All RP columns resolved the 3 analytes. In the Zorbax SB-CN analysis (Figure 1b, Table S3, Entry 1), the PEG-*b*-PLA peak was broad, peakwidth at half-height = 0.90 min, likely due to restricted diffusion since the column is packed with fully porous particles (FPPs) with a pore size of 80 Å.[37] The PEG-*b*-PLA peak became narrower by switching to a 300 Å C8 FPP column (Figure 1b). However, the retention/absorption of the HPMC-C_{12} and PEG-*b*-PLA by the C8 stationary phase was strong and led to a low recovery for both polymers (Table S3, Entry 2), and the sharp PEG-*b*-PLA peak was caused by only a small portion of analyte eluted. Halo C4 400 and 1000 Å columns packed with superficially porous particles (SPP) and less hydrophobic phases were tested to improve the mass transfer kinetics and recovery. Both C4 columns improved recovery of HPMC-C_{12} and provided better resolution between bimatoprost and HPMC-C_{12} compared to SB-CN and SB-C8 columns, while producing reasonable peak shape and recovery for the PEG-*b*-PLA, especially the C4 400 Å column (Table S3, Entry 3, 4). While the C8 300 Å and C4 400 Å columns tested have similar pore sizes, they showed significant differences in recovery, indicating the stationary phase chemistry and particle technology played a key role in improving recovery. Therefore, C4 SPP columns were pursued for further optimization.

Elution Mechanism Discussion and Method Optimization. Due to the kinetically favored PEG-*b*-PLA aggregation in the sample diluent (25−50% MeCN in H_2O), the PEG-*b*-PLA was injected as-is in the NP state (Figure S2a). The starting gradient of 5% MeCN, was not a thermodynamically good solvent for dissolving the NPs, so the injected NPs remained intact. When the pore size is much larger compared with the NP size, the NPs could enter, precipitate and partition into the pores, operating in an interaction/adsorption mode.[38] When the pore size was similar to the NP size, the NPs could be partially excluded from the pore volume, operating with a hybrid mode of exclusion and interaction. As the gradient increased to ~95% MeCN, the nanoparticles were destabilized on column and disrupted into individual PEG-*b*-PLA polymers (Figure S2b). The high organic condition balanced out interactions between individual polymers and the stationary phases; thus, the polymers moved quickly on the column and eluted. The on-column dissociation of NPs was confirmed by coupling RPLC with the MALS detector, revealing the PEG-*b*-PLA peak Mw = 31 kDa (Figure S3), corresponding to polymers instead of NPs (Mw = 11−23 MDa). This on-column dissociation−desorption−elution mechanism was likely responsible for the higher carryover observed in the 1000 Å column compared with the 400 Å column (23.0% to 6.2%, respectively), due to the higher probability of NPs (diameter = 31 nm) partitioning into the 1000 Å pores, leading to slower dissociation of the NPs and desorption of the polymers, causing more carryover.

To further understand this phenomenon, we conducted a study to evaluate the effect of the temperature and pore size on carryover (Table 1). Increasing temperature will accelerate mass transfer and absorption/desorption rates as a result of decreased mobile phase viscosity and increased analyte diffusivity. This led to reduced carryover at elevated temperatures in both 1000 and 400 Å columns (<2% above 50 °C).[38,39] However, the temperature mainly accelerated the desorption-elution stage. The PEG-*b*-PLA did not fully elute when the mobile phase strength was reduced to lower organics (98% to 50%), while it was maintained at 60 °C (Figure S4). The high organics eluent was critical to dissociate the NPs and a higher temperature facilitated the desorption and elution of

https://doi.org/10.1021/acs.analchem.3c05747
Anal. Chem. XXXX, XXX, XXX−XXX

Table 1. Effect of Separation Temperature on the Carryover % of PEG-*b*-PLA

	carryover (% area/area)[a]			
pore size	30 °C	40 °C	50 °C	60 °C
1000 Å	23.0%	7.2%	<2%	<2%
400 Å	6.2%	6.4%	<2%	<2%

[a]Carryover% was determined by the ratio of the PEG-*b*-PLA peak area in the subsequent blank injection and the preceding PEG-*b*-PLA standard injection.

the polymers to reduce carryover. Considering the 400 Å column has a lower likelihood of NPs partitioning into the pores compared with the 1000 Å column, the 400 Å column was selected in the final method.

When the thermostat temperature was increased to 50 °C, the peak shape and height for HPMC-C_{12} was not significantly improved, and we instead observed an increase in retention (Figure S5a,b). This can be explained by the temperature dependent gelation of HPMC. As temperature increases, HPMC starts to lose its water shell, accompanied by an increase in polymer−polymer or polymer−stationary phase interactions.[40,41] A previous study reported gelation started at ∼26 °C, but the onset temperature can vary depending on the composition and functionalization of HPMC.[41] To mitigate the impact of on-column gelation on the separation while maintaining good recovery for PEG-*b*-PLA at 50−60 °C, an eluent step-gradient was implemented to elute the HPMC-C_{12} and improve its on-column solubility (∼80% MeCN) (Figure S5c). The sharpened HPMC-C_{12} peak suggested that the on-column absorption had been alleviated and resulted in a fast elution. The sensitivity of the HPMC-C_{12} improved ∼5 fold compared to the initial linear gradient program.

Diluent Study. To enable quantitative analysis of the intact PNP-2-10 hydrogel by RPLC-CAD, various diluents and sample extraction protocols were adapted to the hydrogel analysis, and their extraction efficiencies were compared. Extraction efficiency was determined by the ratio of the calculated amount of polymer from the RPLC-CAD calibration curve to the theoretical amount of polymer in the intact PNP-2-10 hydrogel. Both a 1-step dilution (gel dissolved as-is in the diluent) and a 2-step dilution (gel dissolved in the organic portion first, followed by the aqueous portion) were assessed (Figure 2). Organic solvent was essential to effectively disrupting the hydrophobic interactions between HPMC-C_{12} and PEG-*b*-PLA NPs. In an aqueous-only diluent, the extraction efficiency for both HPMC-C_{12} and PEG-*b*-PLA NPs was lower than 30%. The 1-step and 2-step dilutions were performed with MeCN/H_2O (25%/75%, v/v) instead of MeCN/H_2O (50%/50%, v/v) due to the peak splitting observed for bimatoprost with the latter diluent. The 1-step dilution showed more variation between duplicate preparations (data not shown). In contrast to 100% MeCN (first extraction solvent in the 2-step dilution), the reduced solvent strength of the 1-step dilution (25%/75% MeCN/H_2O) could not effectively disrupt the hydrophobic interactions between the PEG-*b*-PLA NPs and HPMC-C_{12} nor fully solvate the NPs, leading to insufficient extraction and more variation in the quantitation. Two other solvents THF/H_2O (50%/50%, v/v) and DMSO/H_2O (50%/50%, v/v) were assessed in the 2-step preparation procedure, considering that THF and DMSO have good solubility for the PEG-*b*-PLA NPs. However, DMSO/H_2O showed poor extraction for both components. Although THF/H_2O showed better extraction compared to DMSO/H_2O, ultimately, the 2-step diluent MeCN/H_2O (25%/75%) was selected for the final procedure based on (1) better extraction efficiency for both polymeric components, achieving 90−110% of the theoretical value in the PNP-2-10 hydrogel (Figure 2) and (2) reduced solvent incompatibility that caused peak splitting for the hydrophilic cargo bimatoprost.

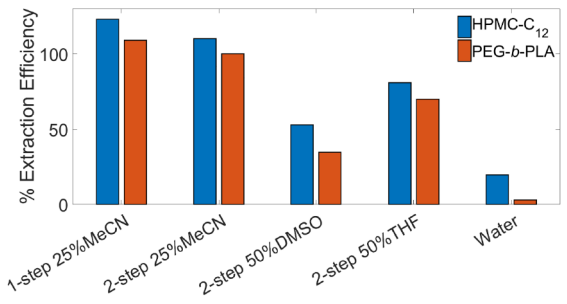

Figure 2. Extraction efficiency% of HPMC-C_{12} and PEG-*b*-PLA NPs (n = 2) from the intact PNP-2-10 hydrogel with various diluents and sample extraction protocols.

Method Performance. The final RPLC-CAD method temperature was set at 60 °C to reduce carryover for PEG-*b*-PLA with the step-gradient for improved HPMC-C_{12} peak shape. The method performance was validated for specificity, linearity, precision, accuracy, and LOQ following ICH Q2 guidance (Figure 3). Method specificity was demonstrated by no interference in the diluent blank affecting the quantitation of PNP-2-10 hydrogel (Figure 3a), as well as a forced degradation study by treating the mixture of HPMC-C_{12} and PEG-*b*-PLA NPs with acid (0.1 M HCl), base (0.1 M NaOH), or heat (60 °C) stressed conditions for ∼20 h (Figure 3b). Following stressed conditions, a common degradant was observed eluting at ∼6 min (before the HPMC-C_{12}). The degradant was formed most rapidly in the base stressed condition, accompanied by a loss of the PEG-*b*-PLA peak, likely associating it with the remaining PEG blocks after PLA blocks hydrolyzed (See Polymer Degradant Characterization by RPLC-MS Section). The method precision was determined by the %RSD of three replicate injections at 10%, 100%, and 120% of the nominal sample loading. Each set of replicates has a %RSD lower than 3.0%, suggesting excellent method precision (Figure 3c). The accuracy of the method was within 90−110% (Figure 3c), red line range) for all components at 10, 100, and 120% of the nominal loading level. Finally, since one application of this CAD method was to study the *in vitro* release of the encapsulated cargo and matrix polymers, the method's working range was validated spanning 3 orders of magnitude for each component in the PNP-2-10 hydrogel and fit with a second order polynomial equation. The polynomial fit was used for calibration to improve method accuracy compared to a linear fit due to the short linear response range of CAD. Over the validated range for each analyte (specified in the Experimental Section), the correlation coefficient was >0.9999 for all three components (Figure 3d−f). The LOQ level was established at 0.03 μg for HPMC-C_{12}, 0.01 μg for PEG-*b*-PLA NPs, and 1 ng for bimatoprost with sufficient sensitivity for *in vitro* release analysis.

The method can be generalized to hydrogels encapsulating other payload types, demonstrated by the separation of a model protein (BSA) from PEG-*b*-PLA and HPMC-C_{12} (Figure S6). Given that the cargo bimatoprost (LogP 3.2)

https://doi.org/10.1021/acs.analchem.3c05747
Anal. Chem. XXXX, XXX, XXX−XXX

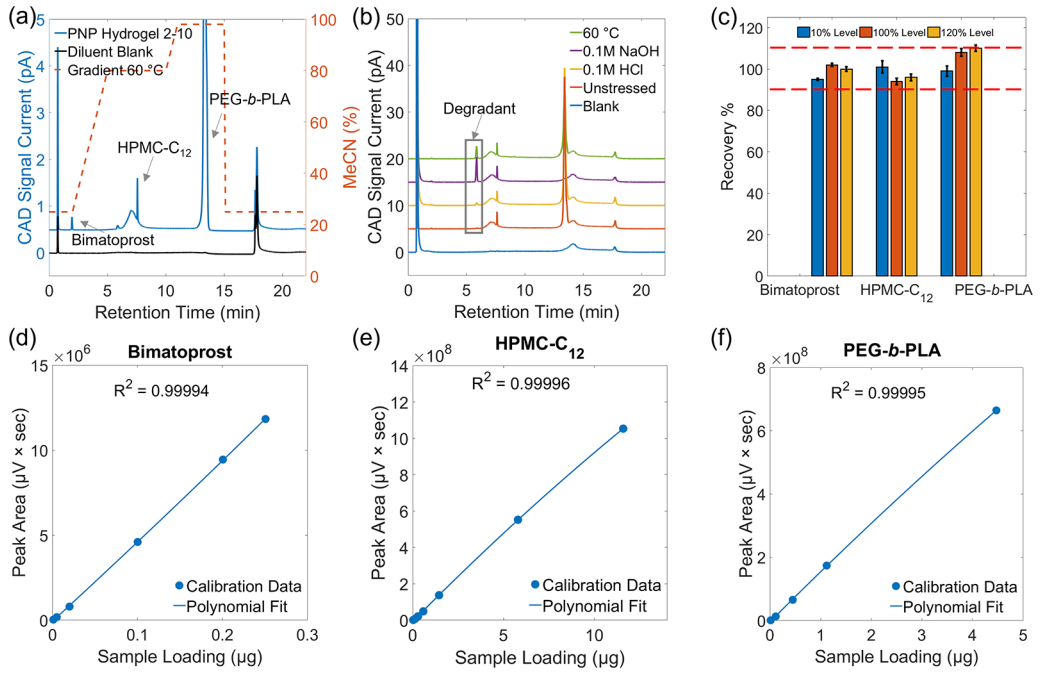

Figure 3. Final RPLC-CAD method chromatograms and performance. (a) RPLC-CAD chromatograms of the intact PNP-2-10 hydrogel (blue) and diluent blank (black), and final method gradient program (orange); (b) forced degradation study of the HPMC-C_{12} and PEG-*b*-PLA NPs; (c) method accuracy by recovery% (n = 3) and precision assessment by RSD%(n = 3) at each concentration; Red line marked the target range of recovery%, 90−110%. The error bar represents standard deviaton. Calibration data and polynomial fitting results for (d) bimatoprost, (e) HPMC-C_{12}, and (f) PEG-*b*-PLA.

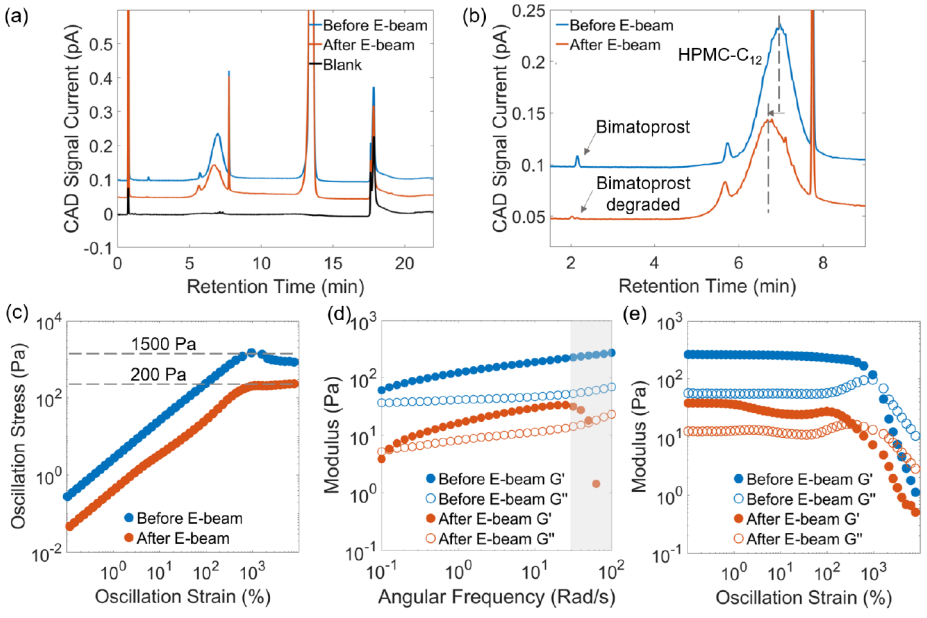

Figure 4. Characterization of hydrogels before and after E-beam sterilization. (a) Chemical composition analysis by the RPLC-CAD method; (b) zoomed in chromatogram highlighted the degradation of bimatoprost and the retention time shift of HPMC-C_{12}; (c) strain−stress characterization; Modulus characterization by (d) frequency sweep and (e) amplitude sweep. The shaded data in (d) were instrument artifacts.

represents the hydrophobicity of most small molecule therapeutics and the C4 column is developed for analytes such as proteins and antibodies; this RPLC method should be suitable for analyzing hydrogels encapsulating a variety of synthetic and biological molecules.

Application of the RPLC-CAD and RPLC-MALS Method in Process Development. One application of this method was to monitor the concentrations of two polymeric components and bimatoprost during an *in vitro* release study, which was included in our previous publication using an USP 7 dissolution apparatus.[26] The RPLC-CAD method was applied here to evaluate the compatibility of E-beam sterilization with the hydrogel. E-beam sterilization is a common sterilization process for injectable formulations, involving continuous flow of high energy electrons into the treated materials.[42] However, the E-beam may lead to polymer/cargo degradation and

https://doi.org/10.1021/acs.analchem.3c05747
Anal. Chem. XXXX, XXX, XXX−XXX

impact rheological properties in the case of hydrogel formulations. PNP-2-10 hydrogels with and without E-beam treatment were assessed by the RPLC-CAD method. After E-beam treatment (dose range of 23−27 kGy), the bimatoprost was found to be degraded as evidenced by its earlier elution in the sterilized hydrogel, and its concentration was below the method's detection limit (1 ng) (Figure 4a,b). It is also noteworthy that the HPMC-C_{12} peak apex eluting time shifted earlier from 6.97 min in the control gel to 6.78 min in the E-beam treated gel, signifying a loss of hydrophobicity and degradation of the polymer after sterilization (Figure 4b). To further probe the degradation of the HPMC-C_{12}, the RPLC method was coupled to the MALS detector for inline Mw analysis, which revealed that the HPMC-C_{12} light scattering peak area reduced ∼2 fold after E-beam sterilization (Figure S7). Since the light scattering signal is proportional to Mw, with the analyte's mass concentration and dn/dc values remained the same, the MALS results suggested the HPMC-C_{12} Mw reduced ∼2 fold due to E-beam treatment.[43] Such polymer degradation affects the rheological properties of the hydrogel. Oscillatory shear rheology showed altered viscoelastic properties for the hydrogel following E-beam treatment, consistent with the RPLC-CAD results, suggesting gel component degradation. An amplitude sweep showed that the E-beam treated hydrogel had a lower yield stress of 200 Pa compared with the untreated hydrogel's 1500 Pa (Figure 4c). Both the angular frequency and the amplitude sweep showed the sterilized hydrogel had an order of magnitude lower moduli (Figure 4d,e) and a G′ G″ crossover point at a lower strain (Figure 4e), indicating that the hydrogel became less stiff after E-beam irradiation. This study demonstrated the RPLC-CAD method provided chemical stability information for the hydrogel and assessed the impact of the manufacturing process on the product quality. Importantly, the RPLC-CAD method can establish structure−property relationships by capturing the chemical changes and connecting those changes with the rheological or other mechanical properties of the hydrogels.

Polymer Degradant Characterization by RPLC-MS. As CAD and MS detectors both require volatile buffers as the mobile phase, the RPLC-CAD method was readily transferable to an RPLC-MS system for higher resolution structural elucidation. Here, we probed the identity of the degradant observed in the earlier forced degradation study, particularly under the NaOH-stressed condition (Figure 3b). This degradant was also present at a low level in the intact hydrogel (Figure 3a). The mass spectrum of this degradant was collected in a qTOF mass spectrometer and processed using iFAMS.[27−31] In brief, polymer mass spectra consist of peak distributions with periodic spacing based on the mass of the repeated subunit and the polymer's net charge ($\Delta m/z$), which can be separated by Fourier transform and normalized for charge to yield much simpler mass reconstructions from multiply charged ion populations (Figure 5). The iFAMS deconvolution process, further detailed in Figure S8 revealed that the chromatographically observed degradant is comprised solely of 4.5−6 kDa polymer with a repeated subunit of 44.05 Da, consistent with the 5 kDa PEG blocks used in the synthesis process for PEG-*b*-PLA copolymers.[26]

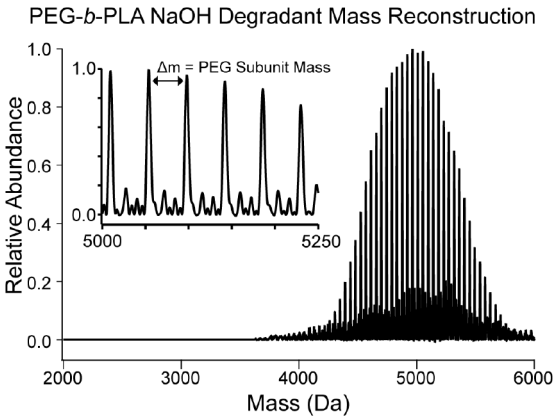

Figure 5. Mass spectral identification of the PEG-*b*-PLA degradant peak from forced degradation study with NaOH. iFAMS mass reconstruction of the 6545XT qTOF polymer degradant spectrum; the inset demonstrates identification of the repeated 44.05 Da PEG subunit.

CONCLUSION

In summary, we presented an RPLC-CAD method as a label-free approach for characterizing CQAs of a supramolecular PNP hydrogel. A reversed-phase C4 400 Å SPP column provided the best specificity and recovery for hydrogel composition analysis. We found that the PEG-*b*-PLA NPs adopted an on-column dissociation-desorption-elution mechanism in the reversed-phase condition, where high organics gradient was critical to disrupt the PEG-*b*-PLA NPs to PEG-*b*-PLA polymers, followed by desorption and elution. Coupling the RPLC method to a CAD detector, the active cargo and the polymeric components can be quantified simultaneously. The RPLC-CAD method was applied to characterize chemical changes of the hydrogels in forced degradation and E-beam studies, showing the method's capability to capture molecular level changes critical for the hydrogel material properties (*i.e.*, rheological properties). In addition, the RPLC method is compatible with several hyphenations: (a) RPLC-MALS for inline molecular weight analysis, which was used to monitor polymer degradation and provide insights into the PEG-*b*-PLA NPs elution mechanism in the reversed-phase condition, and (b) RPLC-MS for high-resolution structural elucidation. With assistance from the iFAMS deconvolution algorithm, the repeating subunit and molecular weight of a polymer degradant were determined from mass spectra.

The PNP-2-10 supramolecular hydrogel was used as the model system in this study. Given the variety of stationary phase chemistries and particle technologies in RP columns and the universal detection of the CAD, it is possible to apply the RPLC-CAD methodology to characterize the CQAs of hydrogels with alternative cargos and gel chemistries. The RPLC-CAD approach is not necessarily limited to supramolecular hydrogels. In the case of chemically crossed-linked hydrogels, the released cargos and the degraded/dissolved gel matrix can still be monitored in the release medium by RPLC-CAD to study the gel degradation kinetics and structures. With suitable sample preparation/enrichment protocols, quantitation of gel polymers *in vivo* is feasible by the RPLC-CAD approach, which is useful for establishing IVIVC. Another implication of this study is to unlock a multi-attribute analysis workflow for hydrogels. Since MALS is a flow through and non-destructive detector, one- or two-dimensional hyphenation of RPLC-MALS with CAD can realize quantitation and Mw tracking in parallel. Overall, this analytical strategy enables the characterization of hydrogel composition, release, and degradation, opening many opportunities such as establishing

https://doi.org/10.1021/acs.analchem.3c05747
Anal. Chem. XXXX, XXX, XXX−XXX

structure−property relationships in hydrogel design, IVIVC, quality control, and clinical translation of hydrogel therapeutics.

■ ASSOCIATED CONTENT

Supporting Information

The Supporting Information is available free of charge at https://pubs.acs.org/doi/10.1021/acs.analchem.3c05747

Supporting Information includes additional experimental details, MALS, DLS, iFAMS details, and chromatograms (PDF)

■ AUTHOR INFORMATION

Corresponding Authors

Shijia Tang − *Synthetic Molecule Pharmaceutical Sciences, Genentech, Inc., South San Francisco, California 94080, United States;* orcid.org/0000-0002-5303-4293; Email: tang.shijia@gene.com

Eric A. Appel − *Department of Materials Science and Engineering, Stanford University, Stanford, California 94305, United States;* orcid.org/0000-0002-2301-7126; Email: eappel@stanford.edu

Authors

Zachary Pederson − *Synthetic Molecule Pharmaceutical Sciences, Genentech, Inc., South San Francisco, California 94080, United States*

Emily L. Meany − *Department of Bioengineering, Stanford University, Stanford, California 94305, United States;* orcid.org/0000-0001-9060-1253

Chun-Wan Yen − *Synthetic Molecule Pharmaceutical Sciences, Genentech, Inc., South San Francisco, California 94080, United States;* orcid.org/0000-0002-8222-335X

Andrew K. Swansiger − *Department of Chemistry and Biochemistry, University of Oregon, Eugene, Oregon 97403, United States;* orcid.org/0000-0002-7320-5491

James S. Prell − *Department of Chemistry and Biochemistry, University of Oregon, Eugene, Oregon 97403, United States;* orcid.org/0000-0002-7505-9168

Bifan Chen − *Synthetic Molecule Pharmaceutical Sciences, Genentech, Inc., South San Francisco, California 94080, United States;* orcid.org/0000-0003-0379-0821

Abigail K. Grosskopf − *Preclinical and Translational Pharmacokinetics and Pharmacodynamics, Genentech, Inc, South San Francisco, California 94080, United States*

Noah Eckman − *Department of Chemical Engineering, Stanford University, Stanford, California 94305, United States;* orcid.org/0000-0002-4183-0153

Grace Jiang − *Department of Bioengineering, Stanford University, Stanford, California 94305, United States;* orcid.org/0009-0007-5506-5441

Julie Baillet − *Department of Materials Science and Engineering, Stanford University, Stanford, California 94305, United States*

Jackson D. Pellett − *Synthetic Molecule Pharmaceutical Sciences, Genentech, Inc., South San Francisco, California 94080, United States*

Complete contact information is available at: https://pubs.acs.org/10.1021/acs.analchem.3c05747

Author Contributions

[▽]S.T. and Z.P. contributed equally to this work.

Notes

The authors declare no competing financial interest.

■ ACKNOWLEDGMENTS

The authors acknowledged Peter Yehl, Karthik Nagapudi, Dennis Leung, Chris Crittenden, Jessie Ochoa, and Chloe Hu for their management, scientific support and expertise. E.L.M. was supported by the NIH Biotechnology Training Program (T32 GM008412). A.K.S. was supported by the National Science Foundation under award number CHE-1752994 to J.S.P. Scheme and TOC in this manuscript were created with BioRender.com

■ REFERENCES

(1) Appel, E. A.; Del Barrio, J.; Loh, X. J.; Scherman, O. A. *Chem. Soc. Rev.* **2012**, *41*, 6195−6214.

(2) Guvendiren, M.; Lu, H. D.; Burdick, J. A. *Soft Matter* **2012**, *8*, 260−272.

(3) Li, J.; Mooney, D. J. *Nat. Rev. Mater.* **2016**, *1* (12), 1−17.

(4) Rosales, A. M.; Anseth, K. S. *Nat. Rev. Mater.* **2016**, *1*, 1−15.

(5) Tong, X.; Yang, F. *Adv. Healthcare Mater.* **2018**, *7* (7), No. e1701065.

(6) Uman, S.; Dhand, A.; Burdick, J. A. *J. Appl. Polym. Sci.* **2020**, *137* (25), 48668.

(7) Correa, S.; Grosskopf, A. K.; Lopez Hernandez, H.; Chan, D.; Yu, A. C.; Stapleton, L. M.; Appel, E. A. *Chem. Rev.* **2021**, *121*, 11385−11457.

(8) Mann, J. L.; Yu, A. C.; Agmon, G.; Appel, E. A. *Biomater. Sci.* **2018**, *6*, 10−37.

(9) Mandal, A.; Clegg, J. R.; Anselmo, A. C.; Mitragotri, S. *Bioeng. Transl. Med.* **2020**, *5* (2), No. e10158.

(10) Omar, J.; Ponsford, D.; Dreiss, C. A.; Lee, T. C.; Loh, X. J. *Chem. Asian J.* **2022**, *17* (9), No. e202200081.

(11) Wei, L.; Chen, J.; Zhao, S.; Ding, J.; Chen, X. *Acta Biomater.* **2017**, *58*, 44−53.

(12) Hu, C.; Zhang, F.; Long, L.; Kong, Q.; Luo, R.; Wang, Y. *J. Controlled Release* **2020**, *324*, 204−217.

(13) Chen, K.; Wu, Z.; Liu, Y.; Yuan, Y.; Liu, C. *Adv. Funct. Mater.* **2022**, *32*, 2109687.

(14) Artzi, N.; Oliva, N.; Puron, C.; Shitreet, S.; Artzi, S.; Ramos, A.B; Groothuis, A.; Sahagian, G.; Edelman, E. R. *Nat. Mater.* **2011**, *10*, 704−709.

(15) Lai, C. Y.; Wu, P. J.; Roffler, S. R.; Lee, S. T.; Hwang, S. M.; Wang, S. S.; Wang, K.; Hsieh, P. C. *Biomacromolecules* **2014**, *15*, 564−573.

(16) Segovia, N.; Pont, M.; Oliva, N.; Ramos, V.; Borros, S.; Artzi, N. *Adv. Healthc. Mater.* **2015**, *4*, 271−280.

(17) Ma, X.; Sun, X.; Hargrove, D.; Chen, J.; Song, D.; Dong, Q.; Lu, X.; Fan, T.-H.; Fu, Y.; Lei, Y. *Sci. Rep.* **2016**, *6* (1), 19370.

(18) Liu, C.; Bae, K. H.; Yamashita, A.; Chung, J. E.; Kurisawa, M. *Biomacromolecules* **2017**, *18*, 3143−3155.

(19) Kivijarvi, T.; Goksøyr, Ø.; Yassin, M. A.; Jain, S.; Yamada, S.; Morales-Lopez, A.; Mustafa, K.; Finne-Wistrand, A. *Mater. Today Bio* **2022**, *17*, 100483.

(20) Liang, Y.; Hao, Y.; Wu, Y.; Zhou, Z.; Li, J.; Sun, X.; Liu, Y. N. *ACS Appl. Mater. Interfaces* **2019**, *11*, 21381−21390.

(21) Appel, E. A.; Tibbitt, M. W.; Webber, M. J.; Mattix, B. A.; Veiseh, O.; Langer, R. *Nat. Commun.* **2015**, *6*, 6295.

(22) Stapleton, L. M.; Steele, A. N.; Wang, H.; Lopez Hernandez, H.; Yu, A. C.; Paulsen, M. J.; Smith, A. A. A.; Roth, G. A.; Thakore, A. D.; Lucian, H. J.; et al.et al. *Nat. Biomed. Eng.* **2019**, *3*, 611−620.

(23) Roth, G. A.; Gale, E. C.; Alcantara-Hernandez, M.; Luo, W.; Axpe, E.; Verma, R.; Yin, Q.; Yu, A. C.; Hernandez, H. L.; Maikawa, C. L.; et al.et al *ACS Cent. Sci.* **2020**, *6* (10), 1800−1812.

(24) Yu, A. C.; Lian, H.; Kong, X.; Hernandez, H. L.; Qin, J.; Appel, E. A. *Nat. Commun.* **2021**, *12*, 746.

(25) Grosskopf, A. K.; Labanieh, L.; Klysz, D. D.; Roth, G. A.; Xu, P.; Adebowale, O.; Gale, E. C.; Jons, C. K.; Klich, J. H.; Yan, J.; et al.et al *Sci. Adv.* **2022**, *8* (14), No. eabn8264.
(26) Meany, E. L.; Andaya, R.; Tang, S.; Kasse, C. M.; Fuji, R. N.; Grosskopf, A. K.; d'Aquino, A. L.; Bartoe, J. T.; Ybarra, R.; Shelton, A.; et al.etal *Adv. Ther.* **2023**, *6*, 2200207.
(27) Cleary, S. P.; Thompson, A. M.; Prell, J. S. *Anal. Chem.* **2016**, *88*, 6205−6213.
(28) Cleary, S. P.; Li, H.; Bagal, D.; Loo, J. A.; Campuzano, I. D. G.; Prell, J. S. *J. Am. Soc. Mass Spectrom.* **2018**, *29*, 2067−2080.
(29) Cleary, S. P.; Prell, J. S. *ChemPhyschem* **2019**, *20*, 519−523.
(30) Rolland, A. D.; Prell, J. S. *Chem. Rev.* **2022**, *122*, 7909−7951.
(31) Swansiger, A. K.; Marty, M. T.; Prell, J. S. *J. Am. Soc. Mass Spectrom.* **2022**, *33*, 172−180.
(32) Pirok, B. W. J.; Abdulhussain, N.; Aalbers, T.; Wouters, B.; Peters, R. A. H.; Schoenmakers, P. J. *Anal. Chem.* **2017**, *89*, 9167−9174.
(33) Edam, R.; Eeltink, S.; Vanhoutte, D. J. D.; Kok, W. T.; Schoenmakers, P. J. *J. Chromatogr. A* **2011**, *1218*, 8638−8645.
(34) Li, Y.; Shen, H.; Lyons, J. W.; Sammler, R. L.; Brackhagen, M.; Meunier, D. M. *Carbohydr. Polym.* **2016**, *138*, 290−300.
(35) Engel, A.; Ploger, M.; Mulac, D.; Langer, K. *Int. J. Pharm.* **2014**, *461*, 137−144.
(36) Striegel, A. M.; Yau, W. W.; Kirkland, J. J.; Bly, D. D. *Modern size-exclusion liquid chromatography: Practice of gel permeation and gel filtration chromatography*; Wiley, 2009. DOI: .
(37) Wagner, B. M.; Schuster, S. A.; Boyes, B. E.; Shields, T. J.; Miles, W. L.; Haynes, M. J.; Moran, R. E.; Kirkland, J. J.; Schure, M. R. *J. Chromatogr. A* **2017**, *1489*, 75−85.
(38) Uliyanchenko, E.; van der Wal, S.; Schoenmakers, P. J. *Polym. Chem.* **2012**, *3*, 2313−2335.
(39) Antia, F. D.; Horvath, C. *J. Chromatogr. A* **1988**, *435*, 1−15.
(40) Sarkar, N. *J. Appl. Polym. Sci.* **1979**, *24*, 1073−1087.
(41) Greiderer, A.; Steeneken, L.; Aalbers, T.; Vivo-Truyols, G.; Schoenmakers, P. *J. Chromatogr. A* **2011**, *1218*, 5787−5793.
(42) Tohfafarosh, M.; Baykal, D.; Kiel, J. W.; Mansmann, K.; Kurtz, S. M. *J. Mech. Behav. Biomed. Mater.* **2016**, *53*, 250−256.
(43) Rubinstein, M.; Colby, R. H. *Polymer Physiscs*; Oxford University Press: New York, 2003.

https://doi.org/10.1021/acs.analchem.3c05747
Anal. Chem. XXXX, XXX, XXX−XXX